Int. J. Heat Mass Transfer. Vol. 34, No. 10, pp. 2617–2628, 1991
Printed in Great Britain

0017–9310/91 $3.00 + 0.00

Augmented heat transfer in a pin fin channel with short or long ejection holes

T. K. KUMARAN, J. C. HAN and S. C. LAU

Turbine Heat Transfer Laboratory, Department of Mechanical Engineering, Texas A&M University, College Station, TX 77843, U.S.A.

(*Received* 20 *July* 1990 *and in final form* 8 *November* 1990)

Abstract—Experiments are performed to determine the heat transfer, pressure drop, and mass flow rate in a pin fin channel with short or long ejection holes on one of the channel sidewalls. The test section consists of eight copper segments that are individually heated to maintain an isothermal boundary wall condition. The segmentally averaged Nusselt numbers are determined. The heat transfer in the pin fin channel with sidewall ejection flow is about 25–30% lower than that with the straight flow. The length of the sidewall ejection holes does not significantly alter the heat transfer in the pin fin channel for the lengths of the ejection holes considered.

INTRODUCTION

A HIGHER turbine inlet temperature is necessary to improve the thermal efficiency of a gas turbine engine. Modern gas turbines operate at inlet temperatures way above the melting point of high temperature alloys. Hence, the blades need to be internally cooled. It is important that the maximum blade temperatures do not exceed the permissible level. This study focuses on internal pin fin cooling channels at the trailing edge of turbine blades. Figure 1 is a cutaway view of an advanced gas turbine blade. The cooling air enters the pin fin channel at the base of the airfoil. Most of the cooling air exits the pin fin channel through small ejection holes along the edge of the airfoil. A small quantity of air exits through bleed holes at the channel tip (radial direction). The pin fins promote flow turbulence and enhance heat transfer.

Pin fins in turbine internal cooling passages commonly have height-to-diameter ratios, H/D, between 0.5 and 4.0 because of the size of modern gas turbine blades and manufacturing constraints. VanFossen [1] studied heat transfer for several staggered configurations with $0.5 \leqslant H/D \leqslant 2.0$. All arrays had four rows of pins in the streamwise direction. Heat transfer rates were averaged over the four-row array. The overall heat transfer coefficients were lower than those for channels with long tubes. VanFossen claimed that the pins had a 35% higher heat transfer coefficient than the endwalls. Brigham and VanFossen [2] investigated the effect of pin height on array averaged heat transfer. The results show that the array averaged heat transfer is not affected for $H/D < 3$. For $H/D > 3$, the heat transfer increases significantly with an increase in H/D.

Metzger *et al.* [3] studied the local row-by-row heat transfer variation in a staggered pin fin array for $X/D = 1.5$ and 2.5, $S/D = 2.5$, and $H/D = 1.0$. Heat transfer increased in the first few rows, reached a peak value and then slowly decreased to a fully developed value. Metzger and Haley [4] found that streamwise spacing effected the location of the row where the peak heat transfer occurred. They related the local maximum and subsequent decrease in heat transfer with turbulence intensities. The measured turbulence intensities showed a similar peak and decrease in the turbulence level. Simoneau and VanFossen [5] measured the turbulence intensities in a six-row pin fin channel with $H/D = 3.01$ for a staggered array. The results showed that a peak turbulence intensity occurred at the third to fourth row followed by decreasing turbulence to the sixth row. This is consistent with Metzger and Haley's observations. Armstrong and Winstanley [6] summarized prior works on flow and heat transfer in pin fin channels for turbine cooling applications.

Endwall heat transfer in a pin fin array was measured with the naphthalene mass transfer technique [7]. Two smooth duct entrances with lengths of 4 and 21 hydraulic diameters determined how the entrance condition affects the endwall heat transfer. There was no dependence on entrance after the second row. It was shown that the overall heat transfer for a pin fin channel with lateral (trailing edge) ejection holes was lower than that for a channel with no ejection holes [8]. The overall heat transfer and friction factor in a pin fin channel with long or short trailing edge ejection holes was experimentally determined [9]. The overall heat transfer increased when the trailing edge ejection holes were configured to radially force the cooling air downstream before exiting through the trailing edge ejection holes or the tip bleed holes. When the trailing edge ejection holes were long, the overall heat transfer was higher than that in the corresponding short ejection holes. The increase in the overall heat transfer was accompanied by an increase in the overall pressure drop. Saxena [10] studied local heat/mass transfer and pressure drop distributions in a staggered pin fin channel ($S/D = X/D = 2.5$ and $H/D = 1$) with trailing edge ejection holes for $L/d = 2$ and 20. His results showed that the heat/mass transfer coefficients are

NOMENCLATURE

A	surface area of heat transfer in the pin fin channel segments
A_L	surface area of heat transfer in the long ejection segments
A_j	cross-sectional area of the ejection segment
A_{min}	minimum flow cross-sectional area in the pin fin channel
C_p	specific heat of air
d	diameter of ejection holes
D	diameter of pins
f	overall friction factor
f_n	local friction factor in the nth segment of the channel
h_n	heat transfer coefficient in the nth segment of the channel
$h_{L,n}$	heat transfer coefficient in the nth segment of the long ejection holes
H	height of pins
L	length of ejection holes
$LMTD$	log mean temperature difference
$\dot{m}$	total mass flow rate of air
$\dot{m}_{jn}$	rate of mass flow through the nth ejection segment
$\dot{m}_n$	rate of mass flow in the channel at the outlet of the nth segment
$\dot{m}_{xn}$	rate of mass flow in the radial direction at the center of the nth segment
N	number of pin rows in the pin fin channel
Nu_D	Nusselt number based on the diameter of the pins
Nu_d	Nusselt number based on the diameter of the ejection holes
n	number of segments in the pin fin channel or ejection hole
P_{inlet}	inlet pressure
p_{exit}	exit pressure
p_n	local pressure in the nth segment of the channel
q_n	power input to the nth segment in the main channel
$q_{L,n}$	power input to the nth ejection segment
Re_D	Reynolds number based on the diameter of the pin and the maximum velocity
Re_d	Reynolds number based on the diameter of the ejection hole
S	pin spacing in the spanwise direction
T_n	bulk temperature of air at the outlet of the nth segment
T_{jn}	average temperature of air at the inlet of the nth long ejection segment or at the outlet of the nth short ejection segment
T_{jno}	average temperature of air at the outlet of the nth long ejection segment
$T_{s,n}$	average wall temperature of the nth segment in the main channel
$T_{w,n}$	average wall temperature of the nth segment in the long ejection segment
$\bar{T}_n$	bulk temperature of air at the center of the nth segment
X	pin spacing in the radial flow direction.

Greek symbol

ρ	density of air.

high immediately upstream of a pin and in the wake region downstream of a pin. The friction factor increased with an increase in the length of the trailing edge ejection holes and when there were fewer ejection holes.

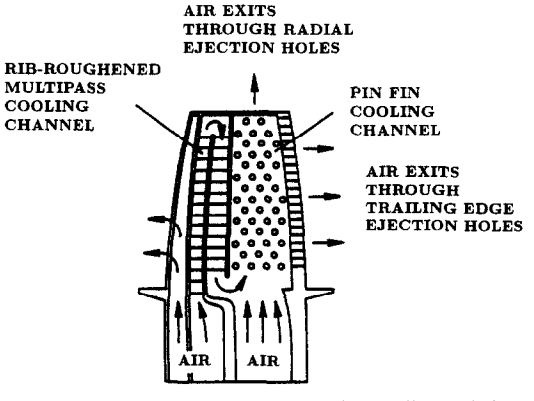

FIG. 1. Cutaway view of a modern internally cooled gas turbine blade.

This study determines the effect of varying the length of the trailing edge ejection holes on the regionally averaged heat transfer coefficient and pressure drop distributions in the pin fin channel. The local radial mass flow rate in the pin fin channel and local mass flow rate in the trailing edge ejection holes are determined for different total mass flow rates. The test section, which is a rectangular pin fin channel, models the trailing edge of a turbine blade and has small lateral ejection holes on one side. The straight flow through the channel simulates the radial flow in a turbine. Heat transfer experiments are conducted by maintaining an isothermal boundary wall condition. Regionally averaged heat transfer coefficients are determined. Heat transfer and pressure drop experiments are conducted for the following test section configurations:

Case 1: straight flow through a pin fin channel with no trailing edge ejection flow and a wide open radial exit;

Case 2: flow through a pin fin channel with 64,

short, trailing edge ejection holes ($L/d = 2$) and five radial exit holes;

Case 3: flow through a pin fin channel with 64, long, trailing edge ejection holes ($L/d = 20$) and five radial exit holes.

For each of the above cases, the flow Reynolds number (based on the pin diameter and maximum flow velocity in the pin fin channel) equals approximately 10 000, 20 000, 30 000, and 50 000. Additional information related to this study can be found in ref. [11].

EXPERIMENTAL APPARATUS

Figure 2 shows the schematic of the test rig, which consists of a gate valve, a calibrated orifice meter, a plenum, an entrance section, and the test section. The air supply is from an air compressor with filters and regulators. The air flow rate is measured with the orifice flow meter constructed to ASME specifications.

Figure 3(a) shows the top view of the pin fin channel for the straight flow case. The test section is a rectangular channel, 50.8 cm (20 in.) long; the cross section measures 9.525 cm (3.75 in.) wide and 1.27 cm (0.5 in.) high and has an aspect ratio of 7.5 : 1. The test section, made entirely of copper, has eight segments. Each segment has two pin rows. The first row has three and the second has two pins. The pin spacing in both the streamwise and spanwise directions is equal to 2.5 times the diameter of the pins, while the height of the pins is equal to their diameter, i.e. $X/D = S/D = 2.5$ and $H/D = 1.0$. Each segment is insulated from its neighbor by balsa wood insulation of 0.1588 cm (0.0625 in.). All segments are aligned and glued together with epoxy. Proper contact is ensured at the joints by applying longitudinal pressure. Checks are made for air leakage in the test section when the segments are glued together.

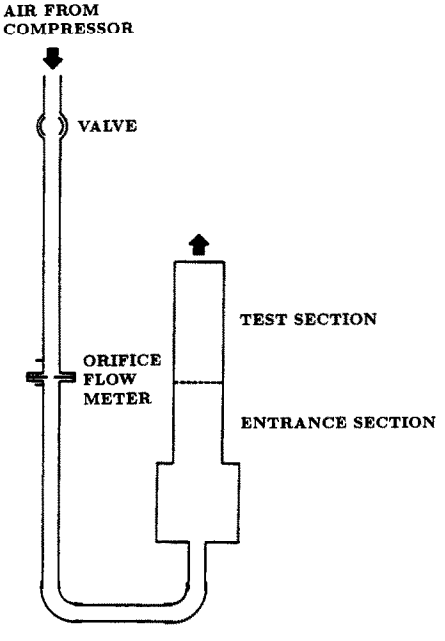

FIG. 2. Schematic of the test rig.

Each segment has four parts—the top wall, bottom wall, and two sidewalls. The pins are press fitted on the top and bottom walls. The pins have a height of 2.54 cm (1 in.). The top and bottom walls are 6.19 cm (2.44 in.) long, 10.80 cm (4.25 in.) wide and 0.64 cm (0.25 in.) thick. The two sidewalls are 6.19 cm (2.44 in.) long, 2.54 cm (1 in.) high and 0.64 cm (0.25 in.) thick. The two sidewalls are bonded to the top and bottom walls with conductive glue. Each complete insulated segment measures 6.35 cm (2.5 in.) long (in the flow direction), 10.80 cm (4.25 in.) wide (in the spanwise direction) and 2.54 cm (1 in.) thick. Figures 3(b) and (c) show the top view of the ejection hole configuration for the short and long ejection hole cases, respectively. One channel sidewall has eight segments. Each segment has eight ejection holes of 0.318 cm (0.125 in.) diameter at equal intervals. Since there are no ejection holes for the straight flow case, Fig. 3(a), this sidewall is a solid flat surface with no holes. The pressure taps, one for each segment, are on the other sidewall in line with the second row of two pins in each segment. An additional pressure tap and thermocouple measure the inlet pressure and air temperature at the end of the entrance section. Two thermocouples measure the temperature of the top wall and one thermocouple measures the temperature of the bottom wall in each segment. The locations of the thermocouples and pressure taps for the straight flow and short and long ejection hole cases are given in Figs. 3(a)–(c), respectively. In each segment, heaters are bonded to the top and bottom walls with epoxy. The two heaters are connected in parallel. Each pair of heaters is connected to the power supply through a transformer. This arrangement enables an isothermal boundary wall condition, where the transformers are adjusted so the wall temperature in all segments is about 54.44°C (130°F). The downstream end of the test section has an endwall with five ejection holes for cases 2 and 3. The endwall is glued to the eighth segment, except for the straight flow case, where the endwall is removed. The whole test section is enclosed by insulation to minimize heat loss to the surroundings.

All pressure taps are connected through a pressure selector switch to an inclined tube water manometer or a U-tube water or mercury manometer, depending on the range. The inclined manometer has a range of 27.9 cm (11 in.) of water and a resolution of 0.254 mm (0.01 in.); the U-tube manometer has a range of 91.4 cm (36.0 in.) of water. A mercury barometer measures the laboratory's atmospheric pressure.

DATA REDUCTION

The equations for reducing the experimental data are given in this section. The definitions of the overall friction factor and the local friction factor, and the

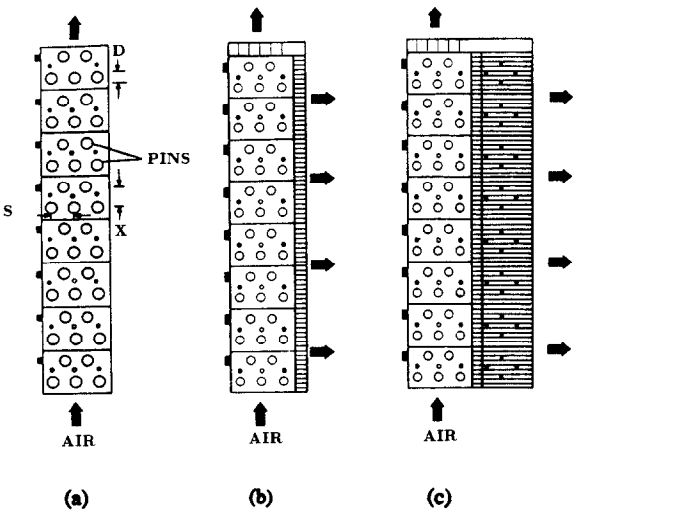

FIG. 3. Schematic of the top view of the pin fin channel: (a) for straight flow—case 1; (b) for short ejection hole flow—case 2; (c) for long ejection hole flow—case 3.

methods to calculate the local mass flow rates in the radial and ejection holes follow those given in refs. [8, 9].

Friction factor and mass flow rates

The total pressure drop across the test section and the local pressure in the test section with respect to the exit pressure are normalized by the dynamic pressure based on u_{max}. The overall friction factor is

$$f = \frac{p_{inlet} - p_{exit}}{\frac{1}{2}\rho u_{max}^2 N} = \frac{2(p_{inlet} - p_{exit})\rho A_{min}^2}{\dot{m}^2 N}. \quad (1)$$

The local friction factor in the nth segment of the channel is

$$f_n = \frac{p_n - p_{exit}}{\frac{1}{2}\rho u_{max}^2} = \frac{2(p_n - p_{exit})\rho A_{min}^2}{\dot{m}^2}. \quad (2)$$

The estimated rate of mass flow through the nth ejection segment is

$$\dot{m}_{jn} = C_D A_j [2\rho(p_n - p_{exit})]^{1/2} \quad (3)$$

where C_D is the discharge coefficient and A_j the flow cross-sectional area of the ejection segment. Each segment has eight holes except the last segment, which has 13. The sum of the rates of mass flow through all eight segments (69 ejection holes) is equal to the rate of total mass flow through the pin fin channel, $\dot{m}$. If the value of C_D does not change significantly from one ejection segment to another, it can be shown that

$$\frac{\dot{m}_{jn}}{\dot{m}} = \frac{f_n^{1/2}}{\sum_{n=1}^{8} f_n^{1/2}}. \quad (4)$$

The ratio of the local radial flow rate to the total mass flow rate is then

$$\frac{\dot{m}_n}{\dot{m}} = 1 - \frac{\sum_{n=1}^{n-1} \dot{m}_{jn}}{\dot{m}} \quad (5)$$

where $\Sigma\dot{m}_{jn}/\dot{m}$ is the sum of the rates of mass flow through the ejection segments upstream of the segment at which the value of $\dot{m}_n/\dot{m}$ is to be calculated. The main channel average mass flow in any segment is the average of the inlet and outlet mass flow in that segment. For the nth segment, it is

$$\frac{\dot{m}_{xn}}{\dot{m}} = \frac{\dot{m}_{n-1} + \dot{m}_n}{2\dot{m}}. \quad (6)$$

The Reynolds number in the pin fin channel based on the pin diameter and maximum velocity is

$$Re_D = \frac{\rho u_{max} D}{\mu} = \frac{\dot{m} D}{A_{min}\mu}. \quad (7)$$

The characteristic length in the Reynolds number is the hydraulic diameter of the channel for the plain channel flow case. In equations (1)–(7), the properties of the flowing air are evaluated at the arithmetic average of the segment and bulk temperature.

Heat transfer coefficients

For the straight flow case, the calculations for Nusselt numbers follow from Metzger *et al.* [3]. Figure 4(a) depicts the location of the variables used in determining the segmental Nusselt number by applying energy balance for each segment. The bulk tem-

perature at the outlet of each segment is calculated based on the inlet temperature of air at the entrance of the segment and the total power supplied to heat the top and bottom walls. From energy balance, the bulk temperature at the outlet of the nth segment is

$$T_n = T_{n-1} + \frac{q_n}{\dot{m}c_p}. \tag{8}$$

Based on inlet and outlet temperatures of air in each segment, a reference temperature ($\bar{T}_n$), corresponding to the center of each segment, is obtained as the arithmetic average of the inlet and outlet temperature of the cooling air. For the nth segment, it is obtained as

$$\bar{T}_n = \frac{T_{n-1} + T_n}{2}. \tag{9}$$

The heat transfer coefficient is

$$h_n = \frac{q_n/A}{(T_{s,n} - \bar{T}_n)} \tag{10}$$

where A is the segmental area exposed to flow (i.e. pins, endwalls, and sidewalls). The Nusselt number based on the pin diameter is

$$Nu_{D,n} = \frac{h_n D}{k}. \tag{11}$$

For convenience, Nu_D is used instead of $Nu_{D,n}$.

For the second case (short ejection holes on one of the channel sidewalls), the mass flow through the main channel of the test section varies because of the ejection of the mass flow through the ejection holes. The mass flow through the nth ejection segment is calculated from equation (4) and the mass flow through the nth main channel from equation (6). Figure 4(b) outlines the location of the variables used in determining the segmental Nusselt number by applying energy balance for each segment. The bulk temperature at the outlet of each segment is

$$T_n = T_{n-1} + \frac{q_n}{\dot{m}_{xn}c_p}. \tag{12}$$

The average temperature of air at the outlet of any ejection segment (T_{jn}) is measured by positioning a thermocouple at the outlet of each ejection hole and measuring the average temperature of the exiting air. The mass flow in each segment splits and becomes either radial flow or sidewall ejection flow. A dummy variable (T_{na}) is defined to obtain a common bulk temperature based on the two streams. For the nth segment it is

$$T_{na} = \frac{\dot{m}_n T_n + \dot{m}_{jn} T_{jn}}{\dot{m}_{n-1}}. \tag{13}$$

The reference temperature ($\bar{T}_n$) for the nth segment is

$$\bar{T}_n = \frac{T_{n-1} + T_{na}}{2}. \tag{14}$$

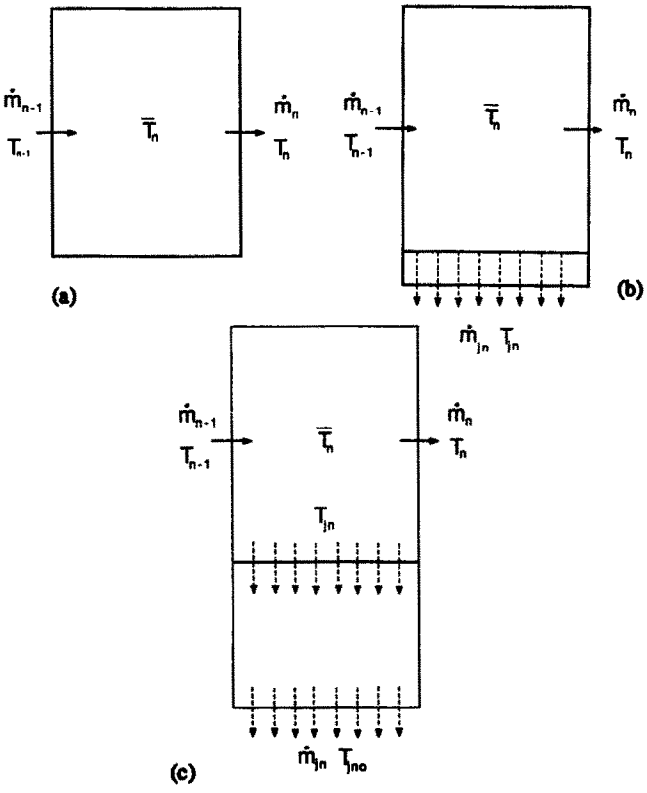

FIG. 4. Schematic for energy balance on any segment: (a) case 1; (b) case 2; (c) case 3.

The heat transfer area (A) in each segment, besides the channel area exposed to flow, includes the eight short ejection holes exposed to flow and the outer sidewall area from which heat is convected by the exiting trailing edge ejection flow. The Nusselt number averaged over each segment is obtained from equations (10) and (11).

For the third case with long ejection holes, besides determining the segmental Nusselt numbers in the main channel as described for the short ejection hole case, the sequential Nusselt numbers in the long ejection hole segments are determined. With the average outlet temperature of air at the ejection holes measured (T_{jno}), the average temperature of air at the inlet of the ejection holes (T_{jn}) can be determined from energy balance. Figure 4(c) outlines the location of the variables used in determining the segmental Nusselt number by applying energy balance. For each ejection hole segment, the average inlet temperature is determined from knowledge of the average outlet temperature from

$$T_{jn} = T_{jno} - \frac{q_{L,n}}{\dot{m}_{jn} c_p}. \tag{15}$$

The log mean temperature difference for the nth ejection hole segment is calculated by

$$LMTD_n = \frac{(T_{w,n} - T_{jn}) - (T_{w,n} - T_{jno})}{\ln \dfrac{(T_{w,n} - T_{jn})}{(T_{w,n} - T_{jno})}}. \tag{16}$$

The Nusselt numbers are determined for the long ejection segments with the log mean temperature difference

$$h_{L,n} = \frac{q_{L,n}/A_L}{LMTD_n} \tag{17}$$

where A_L is the flow area of the long ejection segments

$$Nu_{d,n} = \frac{h_{L,n} d}{k}. \tag{18}$$

For convenience, Nu_d is used instead of $Nu_{d,n}$.

Uncertainty in data reduction

The pressure drop across the orifice in the flow meter fluctuated no more than 2.0% during any of the test runs. It has been concluded, accounting for variations of other parameters, that the uncertainty in the calculation of the mass flow rate is not more than 3.8%. The uncertainties in determining flow area (A) and diameter of pin (D) are estimated to be about 0.8%. The uncertainty in velocity is 4.08%. Applying the Kline and McClintock theory [12], the maximum uncertainty in the calculated Reynolds number and friction factor is about 4.2 and 6.3%, respectively. The power input to the heater with the common 110 V AC supply had a fluctuation of 1.4%. The inlet temperature of the air varied by no more than 0.4%. Hence, for any Reynolds number, the bulk temperature varied by no more than 4.1%. The uncertainty in the wall temperature is estimated to be about 0.8%. The calculated Nusselt number has an uncertainty of 4.6% for any Reynolds number.

RESULTS AND DISCUSSIONS

Heat transfer results

Figure 5 compares the variation of the overall Nusselt number with the Reynolds number on a log–log scale for the straight flow case with that of Metzger *et al.* [3] and Lau *et al.* [9]. An increase in Reynolds numbers results in an increase in Nusselt numbers. The data fall almost on a straight line. Metzger *et al.*'s Nusselt numbers seem to be higher at higher Reynolds numbers when compared to case 1, probably because the geometry of the test section in the present investigation is very different from that of Metzger *et al.* Although the staggered pin arrangement of $X/D = S/D = 2.5$ and $H/D = 1.0$ is the same in all three studies, the test section of Metzger *et al.* had ten rows with ten pins in each row and a 25 : 1 flow cross section. The test section in the present investigation has 16 rows of three and two pins alternately arranged and a flow cross section of 7.5 : 1. The test section of ref. [9] had 15 rows of three pins and a flow cross section of 8.75 : 1. It appears that for the same pin configuration, varying the number of pins per row and the number of rows in the flow direction significantly affects the heat transfer characteristics of the air flow in a pin fin channel. The low overall heat transfer coefficient in the present study is probably because of the smaller flow cross section as compared to Metzger *et al.* [3]. The data from the present study agrees with that of ref. [9] because of comparable channel geometry and an almost equal number of pin rows. The best fit equation for case 1 is

$$Nu_D = 0.298 Re_D^{0.571}. \tag{19}$$

Figure 5 shows the variation of overall Nusselt numbers with Reynolds numbers for the three cases studied. For all three cases, the Nusselt number increases by increasing the Reynolds number. When plotted on a log–log scale, the data fall almost on a straight line. For all cases studied, the heat transfer is lowest for the long ejection hole case. The Nusselt numbers in the pin fin channel with the long ejection holes are lower than the short ejection holes by 5–10%. Compared with the straight flow case, the Nusselt numbers in the pin fin channel with the long ejection holes are 30% lower.

Figure 6 compares row-averaged Nusselt number for the straight flow case with that of Metzger *et al.* [3] for the four Reynolds numbers studied. Metzger *et al.* had ten rows with ten pins in each row and determined Nusselt numbers averaged over every row. The present study determined Nusselt numbers averaged over two rows of pins. Hence Metzger *et al.*'s results were corrected. The corrected Nusselt numbers for the corresponding Reynolds numbers were obtained as the arithmetic average of Nusselt numbers

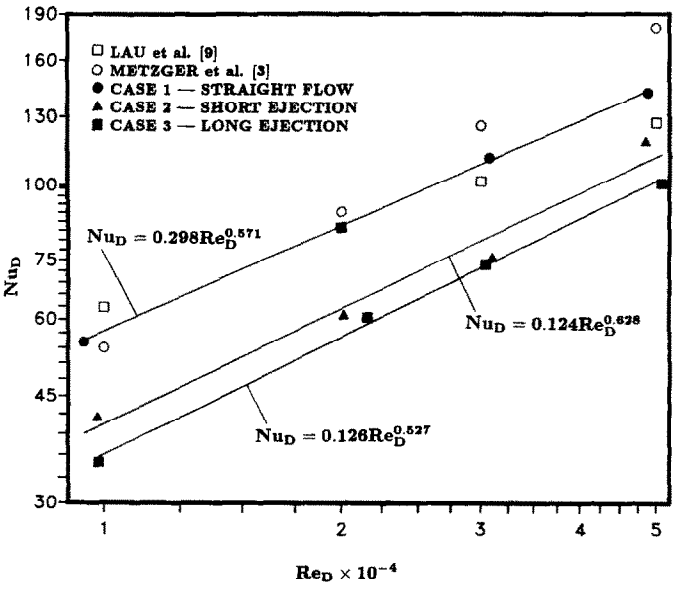

FIG. 5. Variation of overall Nusselt number with Reynolds number: comparison for straight flow and comparison for cases 1–3.

over every two rows. Metzger *et al.*'s results show an increase in Nusselt numbers over the first few rows and then a gradual decrease to a fully developed value. The inlet impingement increases the heat transfer in the first few rows and brings the Nusselt number to a fully developed value in the third or fourth row. The results of the present study for all Reynolds numbers studied are: an increase in Nusselt numbers over the first two segments, remaining almost constant over the next three segments, and a gradual increase from the sixth to the eighth segment. The trend of the data from the sixth to the eighth segment was unexpected. Metzger *et al.* had ten rows of pins while in this study there are 16 rows of pins. The trends in both studies are similar, i.e. corresponding to ten rows of pins, until the fifth segment. No physical explanation can be given for the observed change in trend.

Figure 7(a) shows the variation of Nusselt number for case 2, i.e. with short ejection holes ($L/d = 2$) for Reynolds numbers of 10 000, 20 000, 30 000, and 50 000. The general trend of the data is an increase in Nusselt number in the first two segments, followed by a sharp decrease until the seventh segment. The Nusselt numbers are greater in the eighth segment than in the seventh segment for all Reynolds numbers. This is because of air impingement against the par-

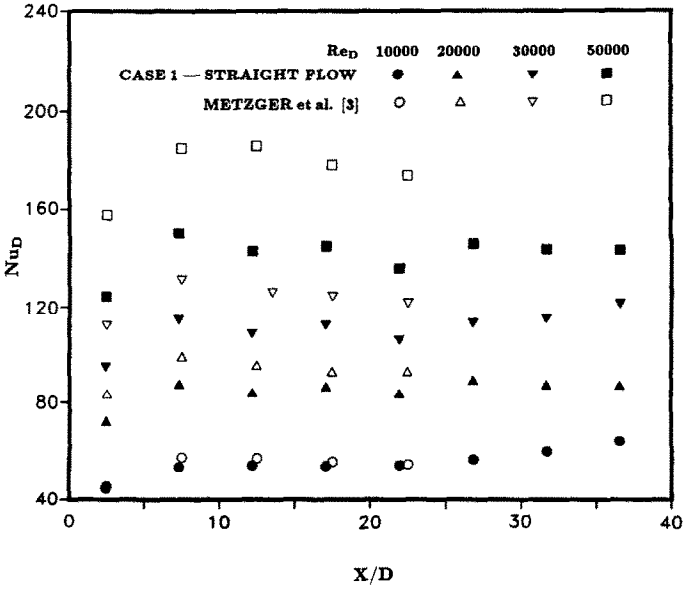

FIG. 6. Comparison of local Nusselt number for straight flow—case 1.

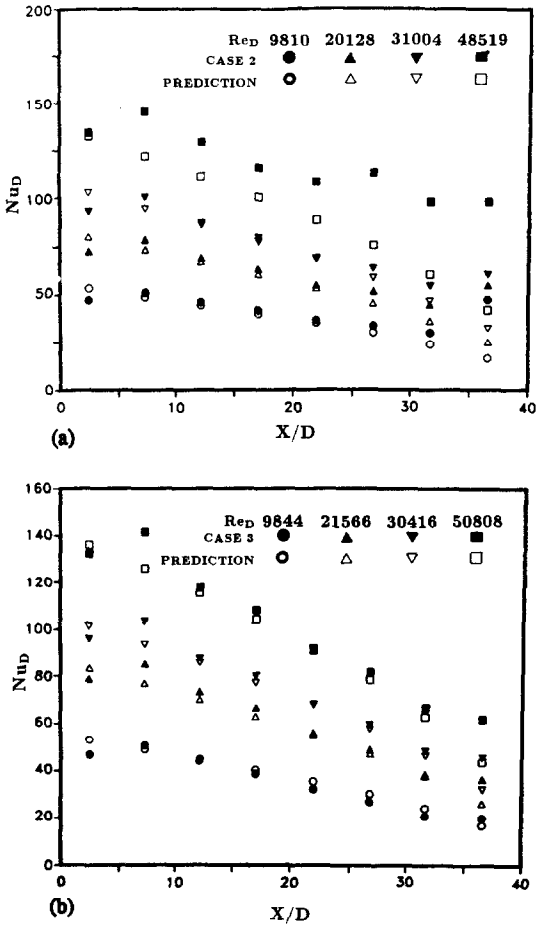

FIG. 7. Comparison between the measured and predicted local Nusselt number: (a) case 2; (b) case 3.

tially blocked radial exit, heat loss by convection, and radiation to the environment. The air exiting the test section in the radial direction escapes through the tip bleed holes and the impingement on the radial exit wall results in higher heat transfer in the eighth segment. The decrease in Nusselt numbers in the radial direction is large because of a decreasing radial mass flow caused by ejection of mass through one of the channel sidewalls. It is evident from Fig. 7(a) that the increase in Reynolds numbers results in an increase in Nusselt numbers.

In applications where the trailing edge cooling of turbine blades is employed, it is common practice to predict the Nusselt number distribution in the pin fin channel with the trailing edge ejection hole by the predetermined Nusselt number distribution in the pin fin channel with the straight flow only for the same pin fin array. This is done by determining the Reynolds number at the desired X/D location for the trailing edge ejection cases (from Fig. 11) and the corresponding Nusselt number from Fig. 5 or the best fit equation (19) for case 1. Figure 7(a) shows the predicted Nusselt numbers. The increase in the Nusselt number in the first and eighth segment cannot be predicted by equation (19) since the effect of impingement on the pins and radial exit wall is not yet quantifiable. However, the decrease in the Nusselt number in the radial direction can be predicted because of its predominant dependence on the Reynolds number. For Reynolds numbers of 10 000, 20 000, and 30 000 the agreement between the experimentally determined and predicted Nusselt numbers is within a maximum 10% in the second, third, fourth, fifth, and sixth segments. For a Reynolds number of 50 000, the agreement between the data and predicted values is poor.

Figure 7(b) shows the variation of the Nusselt number in the radial direction for case 3, i.e. with long trailing edge ejection holes ($L/d = 20$) for the four Reynolds numbers studied. The general trend of the data is an increase in the Nusselt number over the first two segments followed by a sharp decrease until the eighth segment. An increase in Reynolds numbers results in an increase in Nusselt numbers. In this study the heat input to heat the long trailing edge segments was determined separately. It is possible to predict the Nusselt number variation in the channel based on the prediction model as outlined in the preceding discussion. The agreement between the experimentally determined and predicted values is good for all Reynolds numbers. The predicted and experimentally determined Nusselt numbers in the second, third, fourth, fifth, and sixth segments are within a maximum of 10% of each other. The predicted Nusselt number in the first segment is higher than the experimental value by at least 11, 5, and 2.5% for Reynolds numbers of 10 000, 20 000 and 30 000, and 50 000, respectively. The experimentally determined Nusselt number in the eighth segment is higher than that predicted by at least 15 and 27% for Reynolds numbers of 10 000, 20 000, 30 000, and 50 000.

Figure 8(a) shows the variation of Nusselt number in the long ejection segments ($L/d = 20$) for case 3. The general trend is a gradual decrease in Nusselt numbers with increasing radial distance because the ejection mass flow through the long ejection segments decreases along X/D. Figure 8(b) shows the variation of Nusselt numbers for the long ejection segments in case 3 with Reynolds numbers on a log–log scale. Since the flow through the long ejection segments is in the turbulent region, a comparison can be made with the long tube correlation as

$$Nu_d = 0.023 Re^{0.8} Pr^{0.4}. \quad (20)$$

All the data fall on a straight line. It is evident that the heat transfer in the long ejection segments agrees well with the long tube correlation defined by equation (20).

Friction factor and mass flow rate

Figure 9 shows the variation of overall friction factors with Reynolds numbers of 10 000, 20 000, 30 000, and 50 000. With an increase in Reynolds numbers, the overall friction factor clearly decreases. The overall friction factor has a steeper slope than that of

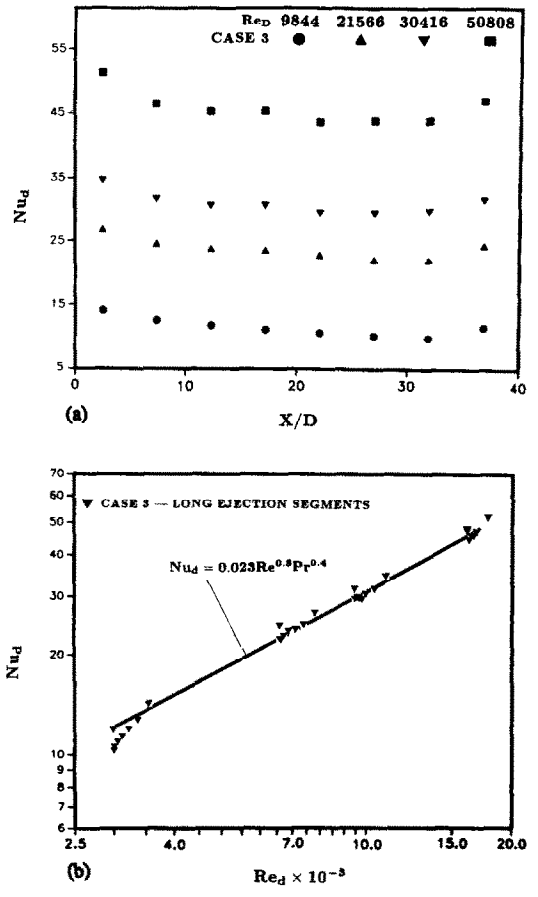

FIG. 8. (a) Variation of local Nusselt number in the long ejection hole segments. (b) Comparison of overall Nusselt number with correlation.

refs. [3, 9], possibly because of the difference in the geometry of the test sections and the arrangement of the pins in the channel. The pressure drop data for the straight flow agrees well with that of Saxena [10] because the geometry of the test section and pin fin arrangement are the same in both studies. Figure 9 also shows the relation between the overall friction factor and Reynolds number for the three cases studied. The long ejection segments create the largest pressure drop in the pin fin channel. Hence, the friction factor is the highest. The slope of the overall friction factor for the straight flow case is large, resulting in a sharp decrease in friction factor with increase in Reynolds numbers.

Figure 10(a) shows the results of local friction factor (normalized local pressure drop) for the straight flow case of the present study for the four Reynolds numbers studied. The local friction factor decreases linearly with increasing distance from the channel entrance. An increase in Reynolds numbers causes a decrease in the local friction factor. Figure 10(b) shows the variation of the local friction factor in the radial direction for the short and long ejection segments. The increased pressure drop as a result of flow resistance in the long ejection segments is evident.

Figure 11(a) shows the variation of the ratio of the ejection mass flow rate to the total mass flow rate along X/D for the short and long ejection segments for the four Reynolds numbers considered. The general trend is a slow decrease in ejection mass flow along X/D. The negative slope near the entrance becomes less negative at the radial exit. The ejection mass flow for the short ejection case is higher at the entrance and lower at the exit for any Reynolds number when compared with the long ejection case. There seems to be no significant effect of Reynolds numbers on the normalized ejection hole mass flow rate for the short and long ejection hole cases. Figure 11(b) shows the variation of the ratio of the radial mass flow rate to the total mass flow rate in the radial direction. Because of ejection of mass flow through the ejection holes, the radial mass flow rate decreases monotonically with increasing distance from the channel entrance. About 10% of the flow exits through the tip bleed holes. There seems to be little difference in the radial mass flow rate between the short and long ejection cases for any Reynolds number, which explains why the overall Nusselt number in the pin fin channel with short and long ejection cases is about the same as in Fig. 5.

CONCLUDING REMARKS

An experimental investigation of turbulent heat transfer in a pin fin channel, with and without lateral ejection holes, studied the effects of varying the Reynolds number, lengths of the lateral ejection holes on the overall pressure drop, local pressure drop, ejection hole mass flow rate, radial mass flow rate, and the segmentally averaged Nusselt number. Results were obtained for a staggered pin fin array with $X/D = S/D = 2.5$ and $H/D = 1.0$ for Reynolds numbers of 10000, 20000, 30000, and 50000. The conclusions are:

(1) The channel cross section and number of pins in the flow direction can significantly affect the overall heat transfer and pressure drop in a pin fin channel with straight flow only.

(2) The segmentally averaged heat transfer in the straight flow case shows an increase in the first two segments, followed by a gradual decrease to a fully developed value. However, the segmentally averaged heat transfer in the case with ejection flow shows an increase in the first two segments then steadily decreases toward the end of the channel. An increase in the Reynolds number causes an increase in the Nusselt number for all the cases studied. The segmentally averaged heat transfer in the straight flow case is always higher than in the case with lateral ejection flow. The heat transfer in the pin fin channel with the lateral ejection flow is not significantly affected by the length of the ejection holes.

(3) A theoretical model predicted the heat transfer distribution in the pin fin channel with short or long ejection holes. The predicted Nusselt numbers agreed

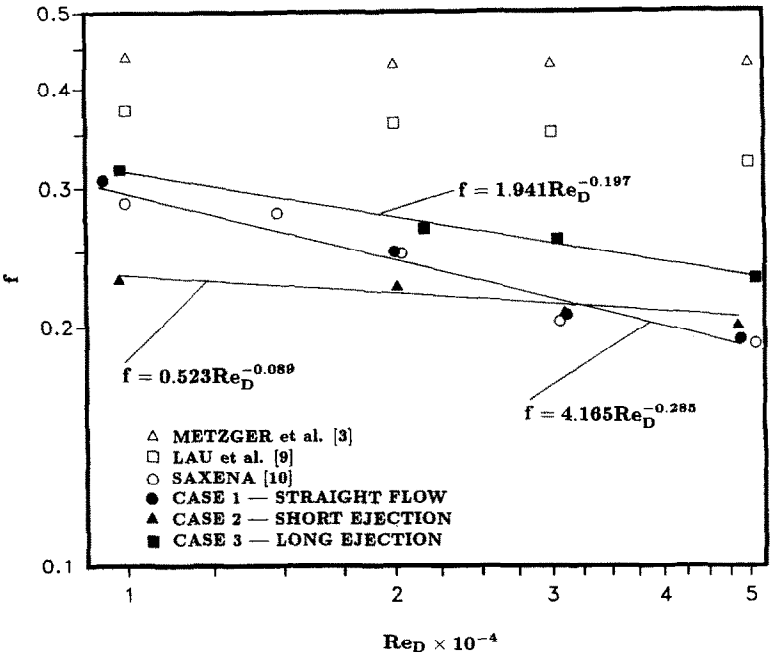

FIG. 9. Variation of overall friction factor with Reynolds number: comparison for straight flow and comparison for cases 1–3.

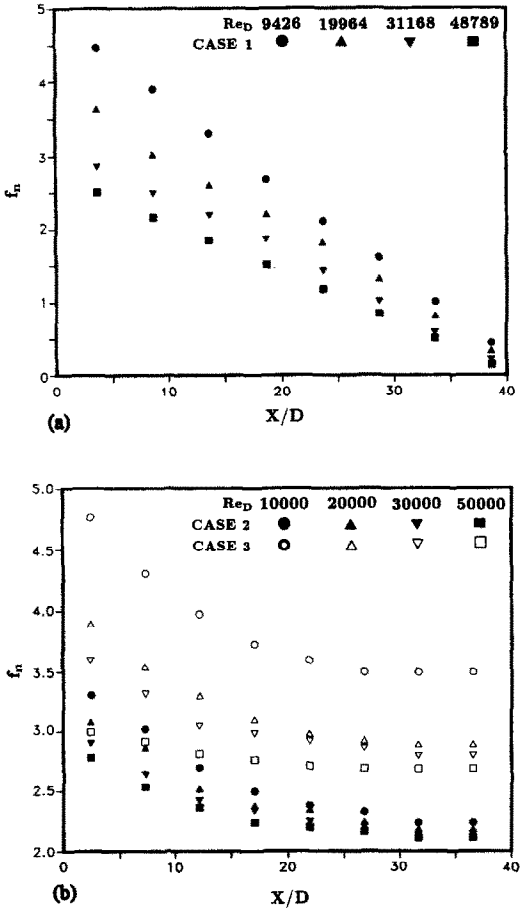

FIG. 10. Comparison of local friction factor: (a) case 1; (b) cases 2 and 3.

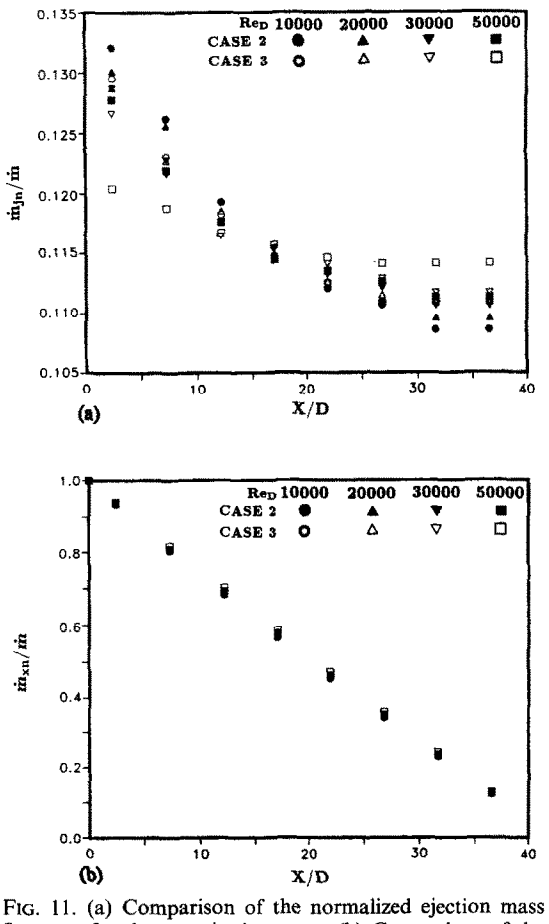

FIG. 11. (a) Comparison of the normalized ejection mass flow rate for the two ejection cases. (b) Comparison of the normalized radial mass flow rate for the two ejection cases.

with experimentally determined Nusselt numbers for both the short and long ejection holes.

(4) For the case with long ejection holes, the heat transfer in the long ejection segments is comparable with the fully developed pipe flow value for all Reynolds numbers studied.

(5) The overall friction factor decreases with increases in Reynolds numbers. The local friction factor decreases gradually in the radial direction for all three cases and for all Reynolds numbers studied. The decrease is linear for the straight flow case and exponential for the short and long ejection cases. For any case, an increase in the Reynolds numbers causes a decrease in the local friction factor.

(6) The ejection mass flow rate decreases from the channel entrance toward the radial exit. The ejection mass flow rate in the short ejection holes is higher near the channel entrance and lower near the radial exit for all Reynolds numbers compared with the long ejection holes.

(7) The radial mass flow rate decreases in the radial direction for all Reynolds numbers. There seems to be little difference in the radial mass flow rate between the cases of short and long ejection holes.

It can be concluded that the straight flow case gives the highest heat transfer in the pin fin channel. However, the trailing edge segment is not cooled at all. If the trailing edge segment is to be cooled, then either short or long edge ejection holes should be used. As a result, the heat transfer in the pin fin channel is reduced by 25–30%. The long trailing edge ejection holes provide heat transfer in the ejection segments and thus effectively cools the tip of the trailing edge. This additional heat transfer in the ejection segments is at the expense of a 3% increased pressure drop in the pin fin channel for low Reynolds numbers and 20% for high Reynolds numbers.

Acknowledgments—This research was supported by the National Science Foundation, grant No. CBT-8713833.

REFERENCES

1. G. J. VanFossen, Heat transfer coefficients for staggered arrays of short pin fins, *ASME J. Engng Pwr* **104,** 268–274 (1982).
2. B. A. Brigham and G. J. VanFossen, Length to diameter ratio and row number effects in short pin fin heat transfer, *ASME J. Engng Gas Turbines Pwr* **106,** 241–245 (1984).
3. D. E. Metzger, R. A. Berry and J. P. Bronson, Developing heat transfer in rectangular ducts with staggered arrays of short pin fins, ASME Paper No. 81-WA/HT-6 (1981).
4. D. E. Metzger and S. W. Haley, Heat transfer experiments and flow visualization for arrays of short pin fins, ASME Paper No. 82-GT-138 (1982).
5. R. J. Simoneau and G. J. VanFossen, Jr., Effect of location in an array on heat transfer to a short cylinder in crossflow, *ASME J. Heat Transfer* **106,** 42–48 (1984).
6. J. Armstrong and D. Winstanley, A review of staggered array pin fin heat transfer for turbine cooling applications, *ASME J. Turbomachinery* **110,** 94–103 (1988).
7. S. C. Lau, Y. S. Kim and J. C. Han, Local endwall heat/mass transfer distributions in pin fin channels, *AIAA J. Thermophys. Heat Transfer* **1**(4), 365–372 (1987).
8. S. C. Lau, J. C. Han and Y. S. Kim, Turbulent heat transfer and friction in pin fin channels with lateral flow ejection, *ASME J. Heat Transfer* **111**(1), 51–58 (1989).
9. S. C. Lau, J. C. Han and T. Batten, Heat transfer, pressure drop, and mass flow rate in pin fin channels with long and short trailing edge ejection holes, *ASME J. Turbomachinery* **111**(2), 117–123 (1989).
10. A. Saxena, Heat transfer and flow characteristics of cooling channels in turbine blades, M.S. Thesis, Texas A&M University, College Station, Texas (1988).
11. T. K. Kumaran, Heat transfer in the trailing edge cooling channels of turbine blades, M.S. Thesis, Texas A&M University, College Station, Texas (1989).
12. S. J. Kline and F. A. McClintock, Describing uncertainties in single-sample experiments, *Mech. Engng* **75,** 3–8 (1953).

TRANSFERT THERMIQUE AMELIORE DANS UN CANAL AVEC PICOTS ET EVENTS D'EJECTION COURTS OU LONGS

Résumé—Des expériences sont conduites pour déterminer le transfert thermique, la perte de pression et le débit-masse dans un canal avec picots et évents d'éjection courts ou longs sur un des côtés du canal. La section d'essai consiste en huit segments de cuivre qui sont chauffés individuellement pour maintenir une condition de paroi isotherme. Les nombres de Nusselt moyennés par segment sont déterminés. Le transfert thermique dans le canal avec éjection pariétale est inférieur de 25–30% au cas de l'écoulement droit. La longueur des trous d'éjection pariétale n'altère pas significativement le transfert thermique dans le canal avec picots pour les longueurs considérées de trou d'éjection.

VERBESSERUNG DES WÄRMEÜBERGANGS IN EINEM NADELRIPPENKANAL MIT KURZEN ODER LANGEN AUSTRITTSÖFFNUNGEN

Zusammenfassung—Es wird der Wärmeübergang, der Druckverlust und der Massenstrom in einem Nadelrippenkanal mit kurzen oder langen Austrittsöffnungen an einer der Kanalseitenwände experimentell untersucht. Die Meßstrecke besteht aus acht Kupfersegmenten, die zur Erzielung einer isothermen Randbedingung an der Wand getrennt geheizt werden können. Die mittlere Nusselt-Zahl für die Segmente wird bestimmt. Der Wärmeübergang in dem Nadelrippenkanal wird durch eine seitliche Zuströmung um ungefähr 25–30% erniedrigt. Die Länge der Austrittsöffnungen wirkt sich im betrachteten Bereich nicht wesentlich auf den Wärmeübergang im Nadelrippenkanal aus.

ИНТЕНСИФИЦИРОВАННЫЙ ТЕПЛОПЕРЕНОС В КАНАЛЕ С ИГОЛЬЧАТЫМ ОРЕБРЕНИЕМ И ОТВЕРСТИЯМИ ДЛЯ ЭЖЕКЦИИ

Аннотация—Экспериментально определяются теплоперенос, перепад давления и массовый расход в канале с игольчатым оребрением при наличии отверстий различных размеров на одной из боковых сторон. Экспериментальный участок состоит из восьми медных сегментов, раздельно нагреваемых для поддержания изотермического граничного условия на стенке. Определяются числа Нуссельта, осредненные по сегментам. Проницаемость боковой стенки уменьшает коэффициент теплопереноса в исследуемом канале примерно на 25–30%. В рассматриваемых случаях размер боковых отверстий не вызывает существенного изменения теплопереноса в канале с игольчатым оребрением.